Facile synthesis of shape-stable phase-change composites via the adsorption of stearic acid onto cellulose microfibers

Denis V. Voronin[*1,2], Rais I. Mendgaziev[1], Kirill A. Cherednichenko[1], Maria I. Rubtsova[1], Polina A. Demina[2], Anna M. Abramova[2], Dmitry G. Shchukin[3], and Vladimir Vinokurov[1]*

1 National University of Oil and Gas «Gubkin University», Moscow 119991, Russia

2 Saratov State University, Saratov 410012, Russia

3 Stephenson Institute for Renewable Energy, Department of Chemistry, University of Liverpool, Liverpool L69 7ZD, United Kingdom

KEYWORDS: Phase change materials, latent heat storage, fatty acids, cyclic stability, thermal degradation, green chemistry, sustainable development

ABSTRACT: Phase change materials (PCMs) offer an exciting way to facilitate energy generation from renewables and develop responsive energy management by storing and releasing thermal energy as latent heat of reversible phase transitions. Organic PCMs are attractive due to their high latent heat storage capacity and reliability. However, they lack shape stability. Here, we propose a simple approach to prepare shape-stable phase-change composite fibers by adsorption of stearic acid onto the surface of cellulose microfibrils. Electron and confocal microscopy demonstrated

that the resultant composites were solely cellulose ribbons 10–15 μm across uniformly covered with a stearic acid layer. Fourier-transform infrared spectroscopy confirmed that stearic acid couples with cellulose by physical adsorption without any surface modification of cellulose fibers. Differential scanning calorimetry showed that the composites have an adjustable latent heat storage capacity of 108–125 J g−1 depending on the mass content of stearic acid (60–70 wt%), which was stable during 20 melting/freezing cycles. The leakage test demonstrated that the confinement of stearic acid onto the cellulose microfibrils prevents its leakage during the solid–liquid phase transition at temperatures comparable to the melting point of stearic acid. Finally, the composite fibers were tested as a thermoregulating additive to a commercially available cement mortar mix.

Introduction

Affordable and clean energy is one of the main goals of sustainable development of modern society[1]. This can be achieved through the rational use of the energy originated from natural non-renewable sources along with the development of energy production from alternative renewable sources[2]. A promising way to facilitate rational energy consumption is the development of responsive energy management implying the accumulation of energy when and where it is accessible and release when and where it is demanded[3]. The thermal energy from natural sources has a great potential for implication in energy management cycles due to its abundance and direct affordability[4]. This requires green technologies for thermal energy storage, transportation, and on-demand release.

Currently, phase change materials (PCMs) are actively studied concerning advanced thermoregulating applications due to their ability to store and release thermal energy as latent heat

(enthalpy) of reversible phase transitions. PCMs are considered as functional additives to construction materials, paints, and textiles. Among others, organic PCMs have advantages of high melting and freezing enthalpies due to the long methylene chains, a wide range of phase transition temperatures, long-term recyclability of latent heat storage, low expansion during melting, absence of supercooling, and chemical inertness[5, 6].

The main issue with organic PCMs is the lack of shape stability that limits their application in a pristine form. To overcome this, encapsulation of organic PCMs in micro- and nanocontainers is typically employed. The micro- and nanoconfined PCMs benefit from the prevention of material exchange with the environment, increased heat transfer area, and improved shape and cyclic stability[7]. The most common approaches in organic PCM encapsulation include reactions of miniemulsion, *in situ,* and interfacial polymerizations[8]. However, in these methods, the resulting properties of encapsulated PCM depend on various synthesis parameters. It is hard to predict their appropriate combination that mostly has to be figured out experimentally, which is time-consuming and not cost-effective.

Alternatively, the shape of organic PCMs can be stabilized by their deposition as a thin layer on some extended surface. The main idea behind this approach is if the PCM layer is thin enough then the coalescence and leakage of the PCM during the phase transition will be prevented by intermolecular interactions with the host surface. Therefore, various fibers with a high specific surface area have the potential to be employed as an adsorbent.

Microfibrillar cellulose (MFC) appears as a promising type of fiber to support organic PCMs. Cellulose is a natural polysaccharide and the most abundant biopolymer on Earth. Micronized cellulose fibrils offer a high mechanical strength () along with a high specific surface area (200 – 250 m^2/g)[9]. The cellulose surface is rich in active hydroxyl groups, which are suitable for chemical

modification[10] and may facilitate the adsorption of PCM molecules. Additionally, it was shown that intramolecular hydrogen bonding and hydrophobic interactions are involved in the formation of cellulose polymeric network that determines its amphiphilic properties and facilitates cellulose interactions with hydrophilic and hydrophobic molecules[11]. Finally, cellulose is a sustainable and cheap biopolymer with a vast base of renewable sources[12].

This work is aimed to demonstrate a fast and simple approach for the preparation of form-stable composite fibrous PCM as exampled by adsorption of organic PCM on the surface of MFC. Stearic acid (SA) was chosen as a model organic PCM due to its suitable phase transition temperature and high latent heat storage ability. Moreover, fatty acids are an attractive type of organic PCM since they can be obtained from renewable sources as well[13]. The composite thermoregulating fibers are promising as functional reinforcing additives to various construction materials and textiles. To date, several thermoregulation fiber compositions were proposed. Generally, they are prepared by chemical grafting of PCM molecules to the fiber surface and demonstrate good shape stability. However, their thermal performance is not high. Therefore, it is of interest to prepare composite thermoregulating fibers by simple adsorption of fatty acid on the MFC and elucidate their thermal behavior, shape stability, and cyclic thermal performance.

Materials and Methods

Materials. The initial raw cellulose materials were provided by Arkhangelsk Pulp and Paper Mill Company (Novodvinsk, Russia). Stearic acid (SA) and Nile Red (NR) dye were purchased from Sigma-Aldrich. These chemicals were used as is without any further purification. Deionized (DI) water (specific resistivity higher than 18.2 MΩ·cm) from a Simplicity UV (Millipore) water purification system was used as an aqueous medium in experiments.

Preparation of MFC. The microfibrillar cellulose was prepared by mechanical treatment of initial raw cellulose pulp. To do this, 5% (wt) aqueous suspension of cellulose pulp was iteratively passed through Masuko Supermasscolloider MKCA6-5 (Masuko Sangyo, Japan) grinder at 6000 rpm for 5 times. Upon this, the resulted MFC mass was dried in a drying chamber (Binder, Germany) at 60°C overnight.

Preparation of SA mixed with NR dye. Stearic acid was mixed with the Nile Red dye to study its distribution in the composites with fluorescent microscopy methods. To do this, 0.7 mg of Nile Red was dissolved in 2 g of melted SA, and then the mixture was further diluted by the addition of the excess of SA. The resulted concentration of the NR dye in the SA was $1.5 \cdot 10^{-4}$ wt%. All experiments on the preparation of SA/MFC composites were carried out with the NR labeled SA, which is further referred to as SA.

Preparation of SA/MFC composites. The SA/MFC composites were prepared by adsorption of SA from melt on the MFC surface. In particular, the portion of SA was melted in the beaker. The portion of MFC was added to the melted SA at a defined weight ratio. After that, the mixture was cooled at 3°C for 10 min, which resulted in the formation of bulk SA/MFC composites. The bulk SA/MFC composites were mechanically grinded once again to restore the cellulose fibrous structure. In this way, the composite fibers containing 60 wt% (SA/MFC 60/40), 65 wt% (SA/MFC 65/35), and 70 wt% (SA/MFC 70/30) of SA were prepared.

Scanning electron microscopy (SEM). The surface morphology of the composite fibers was studied with SEM-FIB JIB-4501 (JEOL, Japan) electron microscope at an accelerating voltage of 10 kV. The fibers were placed on the surface of the conductive carbon tape and sputtered with a 5 nm layer of gold.

Fourier-transform infrared spectroscopy (FTIR) measurements were carried out with Nicolet iS10 (Thermo Scientific, USA) spectrometer with germanium ATR crystal. The absorption model spectra were collected in the 600 – 4000 cm^{-1} range as an averaged result of 16 iterative scans.

Confocal laser scanning microscopy (CLSM) images were captured with a Leica TCS SP8 X (Leica, Germany) microscope equipped with HC PL APO CS 10x/0.40 DRY objective. A 515 nm laser was used to excite the Nile Red fluorescence. The detection was performed in the 560 – 650 nm range.

Differential scanning calorimetry (DSC) was employed to measure the thermal properties and cyclic stability of SA/MFC composites. The measurements were carried out with DSC 214 Polyma (Netzsch, Germany) calorimeter in the range from 20 to 90°C with a heating/cooling rate of 10°C/min. The mass of the samples was 5 mg. The collected DSC data were further time-integrated to calculate the enthalpy of phase transitions in SA/MFC composites employing standard data processing software.

Thermogravimetric analysis (TGA) of the SA/MFC composites was carried out with STA 449 F5 Jupiter (Netzsch, Germany). The data were collected in the range from 30 to 800°C with a heating rate of 10°C/min. The initial mass of the samples was 6 mg. The experiments were carried out under the air atmosphere.

The material leakage test was performed to evaluate the shape-stability of SA/MFC composite fibers. To do this, the portion of SA/MFC sample was placed on the absorbing layer (cellulose paper filter) and heated in the drying chamber for 15 min at the temperature beyond the complete phase transition of SA in SA/MFC composites, which was detected by DSC (see the text below). After that, the samples were cooled at 3°C for 15 min, removed from the absorbing layer, and weighted. The possible SA leakage may be detected as the mass loss by the sample. Totally, 5

iterative heating/cooling cycles during the material leakage test were performed and the mass of the samples was controlled after every heating/cooling cycle.

Results and discussion

Structural characterization of SA/MFC composites

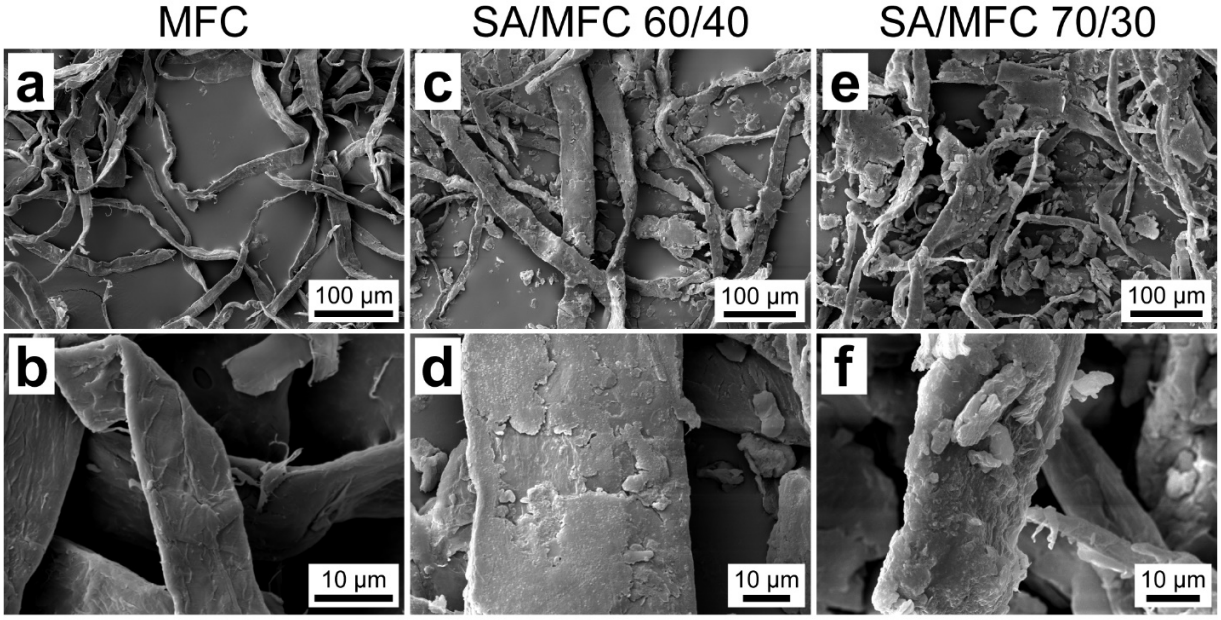

Figure 1. SEM images of the initial MFC (a,b) and the SA/MFC composite fibers prepared by mixing of SA and MFC with a mass ratio of 60/40 wt% (c,d) and 70/30 wt%(e,f) denoted as SA/MFC 60/40 and SA/MFC 70/30 respectively.

At the first set of experiments the structural properties, surface morphology, and composition of prepared fibers were studied. Figure 1 shows the SEM images of the initial cellulose microfibers and those of SA/MFC composites upon regrinding after SA deposition. It is seen that the mechanical grinding of raw cellulose pulp results in MFC with more or less homogeneous ribbon-like fibers with an average lateral length of about 10 – 15 µm (Figure 1a, b). In turn, the images of the SA/MFC samples demonstrate that the composites preserved the fibrous structure (Figure 1c-

f). At the first glance, the covering of the MFC by SA can be recognized by the change of the MFC surface appearance. Comparing to the neat MFC, the surface of the SA/MFC composites have a prominent lamellar morphology, which is formed by the SA deposition. In the case of SA/MFC 60/40 composites (Figure 1c, d), the SA lamellas are uniformly covering the MFC surface. The bigger SA aggregates can be seen on the surface of SA/MFC 70/30 composite fibers (Figure 1e, f). Additionally, free-standing SA particles can be seen as a result of the mechanical treatment of the samples after adsorption of the SA. In the case of SA/MFC 70/30 composite, the amount of free SA is higher, which is related to the higher initial amount of the SA and less available MFC surface for its adsorption.

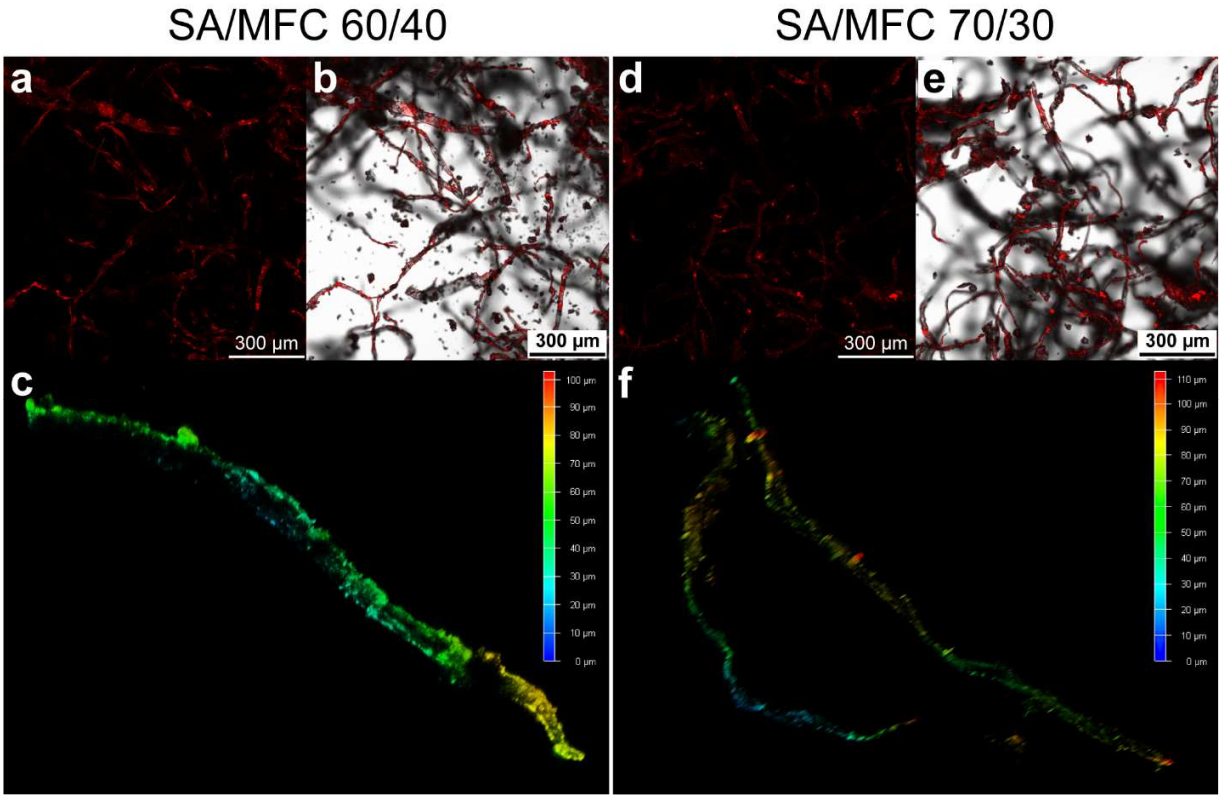

Figure 2. CLSM images of the SA/MFC 60/40 (a-c) and SA/MFC 70/30 (d-f) composite fibers showing the distribution of Nile Red labeled SA onto the MFC surface: (a) and (d) are fluorescent

CLSM images; (b) and (e) are merged fluorescent and transmittance CLSM images; (c) and (f) are 3D reconstructed fluorescent CLSM images.

The adsorption of the SA mixed with NR dye on the surface of the cellulose fibers was additionally confirmed with CLSM measurements. Figure 2a and Figure 2d show the fluorescent images of the SA/MFC fibers captured under excitation by a 515 nm laser. The fluorescent emission follows the shape of the MFC that is also seen on the merged fluorescent and transmission CLSM images (Figure 2b and Figure 2e). The 3D images of the single fibers demonstrate the uniform coating of MFC with SA, which is following the bending of the fibers as it is shown by the color depth coding (Figure 2c and Figure 2d). In addition, some pieces of the free-standing SA can be seen on the transmission images as well.

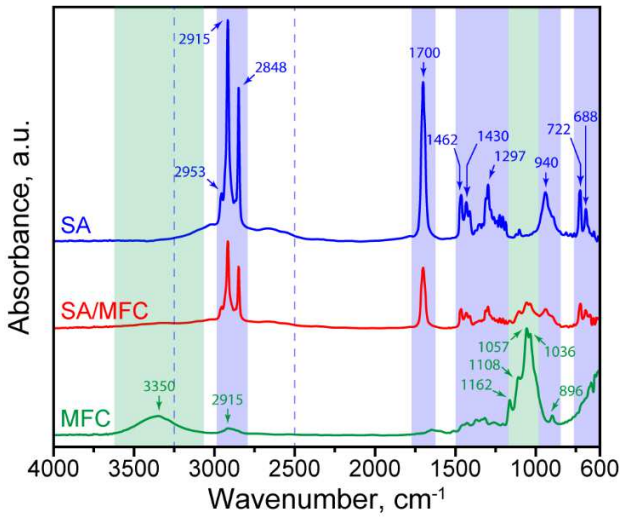

Figure 3. FTIR spectra of SA, MFC, and SA/MFC 70/30 composite fibers. The blue dashed lines mark the envelope corresponding to the stretching vibration of the hydroxyl groups in the SA.

The modification of the MFC surface by SA molecules was studied by FTIR. Figure 3 shows the FTIR spectra of MFC, SA, and SA/MFC 70/30 composite. The FTIR spectra of MFC and SA demonstrate the typical absorption bands with the maximums of absorption corresponding to the

stretching and bending of the inherent functional groups[14, 15]. A detailed description is given in the Supporting Information.

The FTIR spectrum of the modified fibers, as exampled by SA/MFC 70/30 composite, contains the characteristic absorption peaks of both MFC and SA without any shift and the addition of new peaks. This can be attributed to the physical adsorption of the SA molecules on the MFC surface without the formation of new covalent chemical bonds. The possible covalent bonding of cellulose with SA may occur via a reaction of etherification that implies the substitution of hydrogen in cellulose hydroxyl groups with acyl radical of stearic acid[16]. Indeed, the FTIR spectrum of SA/MFC composite demonstrates the absence of absorbance in the 3600 – 3050 cm^{-1} band, whereas the peak at 1700 cm^{-1} related to the stretching of the carbonyl bond remained at the same position as in fatty acids while it should be shifted to ~1750 – 1730 cm^{-1} in cellulose stearate[17]. Further, the SA/MFC spectrum preserves the hydroxyl wagging peak at 940 cm^{-1} and the peaks related to C-OH in-plane bending and C-OH stretching at 1439 cm^{-1} and 1297 cm^{-1}, respectively, indicating the intact hydroxyl group in SA molecules physically adsorbed on the surface. All in all, the results of FTIR spectroscopy accomplish the SEM and CLSM microscopy data and demonstrate the successful modification of MFC with SA.

Thermal properties of SA/MFC composites

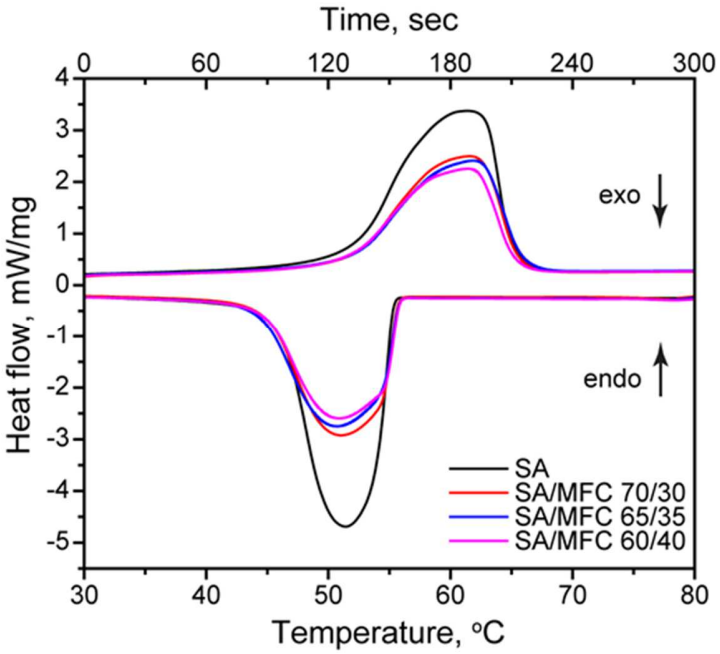

Figure 4. The melting and freezing curves of SA and SA/MFC composites.

Figure 4 shows the DSC curves of pure SA and SA/MFC composites with various mass ratios of SA to MFC. The melting curve of the SA has a single peak at 61.4°C and the melting enthalpy ΔH_M was found to be 177.7 J/g []. The melting points of SA on the surface of MFC remained almost the same as for pristine SA (61.4 – 61.8°C) whereas the melting enthalpy was measured to be lower for all SA/MFC composites (see Table 1).

The DSC data on the melting behavior of PCM in the composite structures can be employed to calculate the PCM loading ratio (R) as

$$R = \frac{\Delta H_{comp}}{\Delta H_{PCM}} \times 100\%, \quad (1)$$

where ΔH_{comp} is the melting enthalpy of the composite, and ΔH_{PCM} is the melting enthalpy of the pure PCM[18]. The loading ratio is one of the important parameters of the composite PCMs. In particular, in SA/MFC composite fibers, the loading ratio indicates the effective performance of SA on the MFC surface to store the heat for thermoregulation. Basing on the above equation the

loading ratio was figured out to be 70% for SA/MFC 70/30, 67% for SA/MFC 65/35, and 60% for SA/MFC 60/40, which is in good agreement with the initial amount of SA added to the MFC.

The freezing curve of SA also has a single peak at 51.5°C along with the freezing enthalpy ΔH_F of 182.1 J/g. Analogous to melting, the freezing enthalpy of the composites reduced to comparing to this of pure SA (see Table 1). Consideration of both melting and freezing enthalpies allows to find out the loading efficiency (E) of SA in SA/MFC composites indicating the heat storage and release performance of the composite fibers towards the pure SA. The loading efficiency can be calculated as

$$E = \frac{\Delta H_{M,comp} + \Delta H_{F,comp}}{\Delta H_{M,PCM} + \Delta H_{F,PCM}} \times 100\% \quad (2)$$

where $\Delta H_{M,comp}$ and $\Delta H_{F,comp}$ are the melting and freezing enthalpies of the SA/MFC composite while $\Delta H_{M,PCM}$ and $\Delta H_{F,PCM}$ are the melting and freezing enthalpies of the pristine SA[18]. The loading efficiency of SA in SA/MFC 70/30, SA/MFC 65/35, and SA/MFC 60/40 composites was found to be 69%, 66%, and 59%, respectively, which gives a more accurate composite thermoregulating performance.

Finally, considering the melting and freezing enthalpies of the SA/MFC composite and those of pure SA, and taking into account the loading ratio, one can calculate the thermal storage capability (η) of the composite fibers as[19]

$$\eta = \frac{\Delta H_{M,comp} + \Delta H_{F,comp}}{(\Delta H_{M,PCM} + \Delta H_{F,PCM}) \times R} \times 100\% \quad (3)$$

The calculated thermal storage capability of SA/MFC 70/30, SA/MFC 65/35, and SA/MFC 60/40 composites was 99%, 99%, and 98%, respectively, which means that almost all SA in the composites can effectively store and release thermal energy through the phase transition. Generally, it is hypothesized that the loading of PCM in restricted volume may affect PCM phase transitions due to confinement effects on their melting and crystallization as exampled by

nanoencapsulated PCM[20]. The values of heat storage capability close to 100% indicate that SA adsorbed on the MFC surface has no confinement restrictions and is free to undergo reversible phase transitions, which is an important prerequisite for heat storage applications. The summary of the thermal properties data collected with DSC is given in Table 1.

Table 1. The summary of thermal properties of SA and SA/MFC composites measured by DSC

Sample	T_M, °C	ΔH_M, J/g	T_F, °C	ΔH_F, J/g	R, %	E, %	η, %
SA	61.4	177.7	51.5	182.1	-	-	-
SA/MFC 70/30	61.5	124.7	51.1	124.5	70	69	99
SA/MFC 65/35	61.8	120.4	50.1	122.7	67	66	99
SA/MFC 60/40	61.4	106.7	50.1	105.9	60	59	98

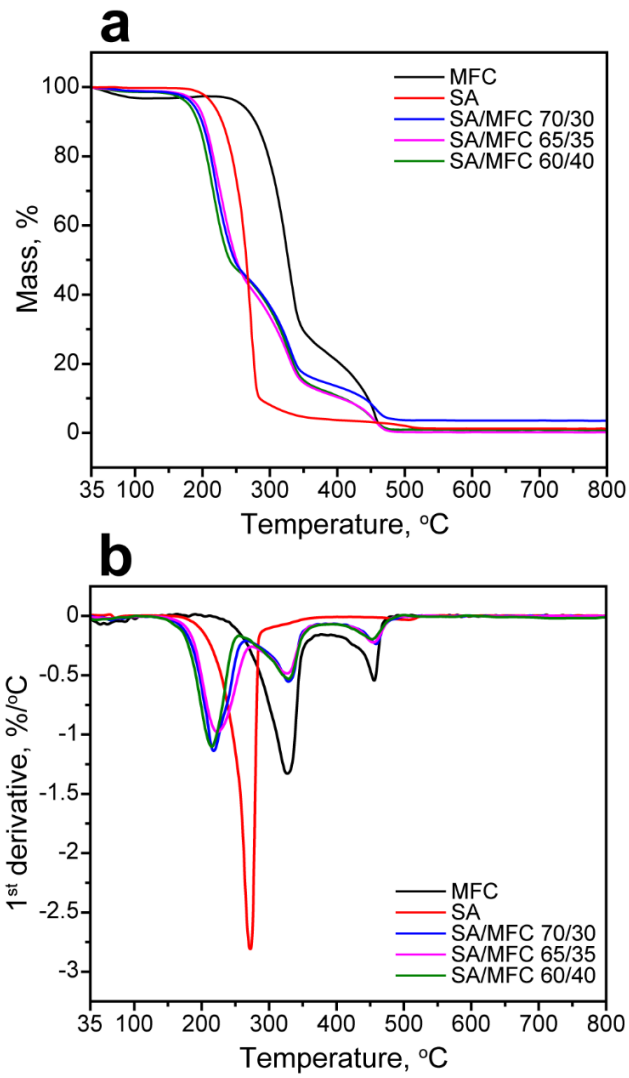

Figure 5. TGA (a) and DTGA (b) curves of MFC, SA, and SA/MFC composites.

The thermal stability of the composite fibers was studied with TGA. Figure 5a shows the results of the TGA analysis of MFC, SA, and the SA/MFC fibers. The TGA curves demonstrate different decomposition patterns depending on the sample type. MFC shows an initial minor weight loss up until 150°C that is related to the evaporation of the bound water []. The onset temperature indicating the beginning of the material degradation is 289°C. The derivatogram (Figure 5b) shows two main decomposition regions from 250°C to 350°C and from 400°C to 500°C with the

inflection points at 327°C and 456°C indicating the temperatures for the maximum rate of decomposition (MRDT) of the amorphous and crystalline regions of the cellulose fibers [21].

The decomposition of SA takes one stage. The onset temperature of pure SA is 246°C while its main decomposition occurs between 220° and 300°C with the MRDT of 272°C.

The thermal decomposition of the SA/MFC composite fibers takes three stages. The composites started to decompose at the onset temperature of 187 – 193°C. The first decomposition stage occurred between 185°C and 250°C with the MRDT at 215 – 222°C. Although the FTIR measurements did not reveal new chemical bonding in the composites, this reminds the thermal degradation behavior of cellulose fatty esters with a very low degree of substitution[22]. In particular, cellulose stearate prepared by etherification of cellulose fibers with a degree of substitution 0.12 (of 3 the greatest possible) demonstrated the onset temperature of 186°C and the MRDT at 207°C. The reduction of thermal stability of cellulose ester compared to initial cellulose was associated with a decrease in cellulose crystalline order due to the partial substitution of cellulose hydroxyls with stearic acid acyls. However, this is unlikely in the case of physical adsorption. Therefore, a decrease in the thermal stability of SA/MFC composites at the first decomposition stage may be related to the faster degradation of SA on the MFC surface. This is confirmed by the presence of the following degradation stages on the derivatograms of SA/MFC composites with the onset temperatures and MRDT similar to those of the MFC degradation. The faster decomposition of SA in SA/MFC composites is due to its confinement on the MFC surface. It is known that the thermal degradation rate constant tends to increase along with a specific surface area of the material, and, therefore, the transition from bulk to fibrillate structure leads to a decrease in the onset temperature and reduced thermal stability[23].

Although the SA/MFC composites were found to have lower onset temperatures in comparison to the pure SA, they remained fairly stable between 35°C and 180°C that meets the thermoregulating range of the composite fibers according to the DSC data. The detailed TGA data are summarized in Table 2.

Table 2. The summary of thermal stability properties of MFC, SA, and SA/MFC composites measured with TGA

Sample	T_{on}, *°C*	*MRDT, °C*	*Residue, %*
MFC	289	327 456	1
SA	246	272	2
SA/MFC 70/30	191	218 329 459	4
SA/MFC 65/35	193	222 327 454	1
SA/MFC 60/40	187	215 329 453	1

Cyclic stability of thermal properties and shape stability

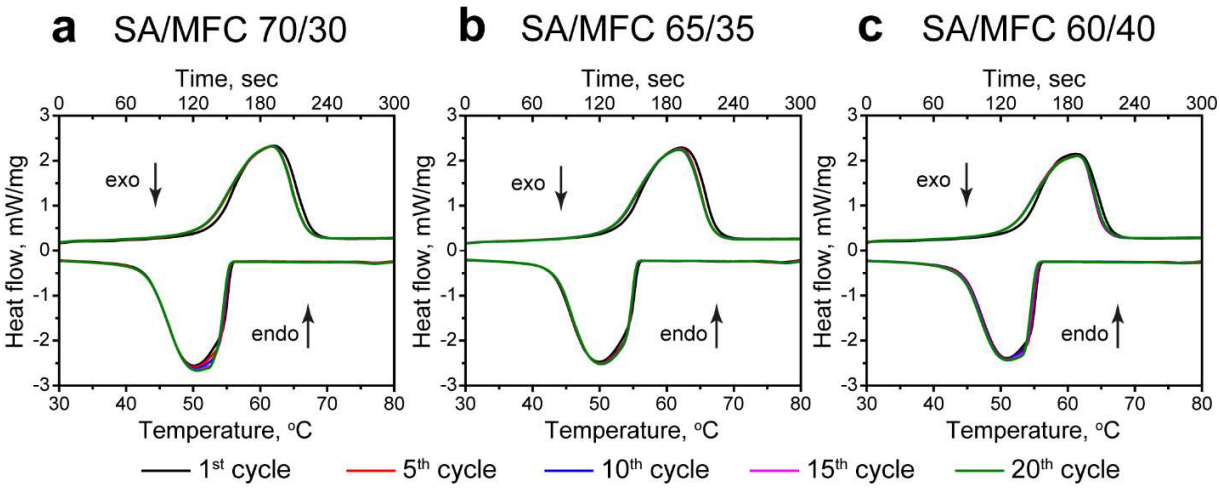

Figure 6. Thermal cycling test of SA/MFC 70/30 (a), SA/MFC 65/35 (b), and SA/MFC 60/40 (c) composites performed by DSC.

At the first step, the cyclic stability of the thermal properties of the SA/MFC composites was studied with DSC. Figure 6 shows the DSC curves of the composite fibers measured within 20 iterative heating and cooling cycles. In general, the DSC analysis did not reveal the substantial changes in the thermal properties of the composites. The comparison of the initial and final DSC curves demonstrates only a slight shift of the melting and freezing temperatures and minor changes in the corresponding enthalpies. The main shift in thermal properties took place after the first heating cycle in all composites and afterward they remained stable. This may be related to the change of the conformation of the SA layer during the melting and crystallization on the MFC surface. All in all, the phase transition temperatures and enthalpies changed non-monotonic depending on the composite structure and the shift value did not exceed 2% for all the samples. The particular values of the melting and freezing enthalpies of the composites calculated from the thermal cyclic stability data measured with DSC are listed in Table 3.

Table 3. The melting and freezing enthalpies of the SA/MFC composites calculated from the thermal cyclic stability data measured with DSC

Sample	*ΔH_M, J/g*					*ΔH_F, J/g*				
	1	*5*	*10*	*15*	*20*	*1*	*5*	*10*	*15*	*20*
SA/MFC 70/30	124.7	122.6	122.4	122.5	122.6	124.5	125	125.2	125.3	125.2
SA/MFC 65/35	120.4	118.1	118.1	117.9	117.9	122.7	120.2	120.3	120.3	120.3
SA/MFC 60/40	106.7	106.7	104.7	104.9	105.1	105.9	107.4	107.2	107.8	108

Although the DSC analysis is a reliable way to study the cyclic thermal stability of the SA/MFC composites, it does not provide any information on the SA leakage from the MFC surface during the phase transition as the measurements are carried out within leakproof Al crucibles. In such a closed system, SA will contribute to the overall DSC signal even if it is leaked from the MFC surface. Therefore, the shape stability of SA/MFC composites was additionally tested by heating the composites on an absorbing material. The possible SA leakage was detected by the measurement of the samples' mass after every heating (and cooling) cycle. Considering the TGA data, the heating temperatures were taken in the range up to 150°C to prevent thermal decomposition. In the first set of experiments, the SA/MFC composites were heated at 75°C, which corresponds to the complete phase transition of the SA according to the DSC melting curves. The SA/MFC 60/40 and SA/MFC 70/30 samples were tested as two representative compositions.

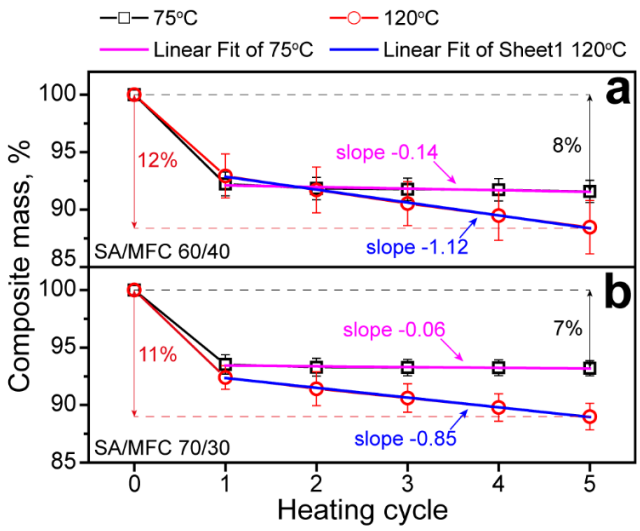

Figure 7. The shape stability test of SA/MFC 60/40 and SA/MFC 70/30 composites.

Figure 7 shows the dependence of the mass change of the SA/MFC 60/40 (Figure 7a) and SA/MFC 70/30 (Figure 7b) composites depending on the number of heating cycles. The most prominent mass loss occurs after the first heating cycle that can be associated with the leakage of the free-standing SA from the samples. Further, the mass of the composites remains stable which can be seen by the negligible slope of the linear fitting curve in the range from the first to the fifth heating cycle. The absolute value of the slope for SA/MFC 60/40 composite is 0.14 while this for SA/MFC 70/30 composite is 0.06. The overall mass loss after 5 heating cycles was found to be 8% for SA/MFC 60/40 composite and 7% for SA/MFC 70/30 composite.

In the next set of experiments, the composites were heated at 120°C to find out if they remain stable after a significant increase in the ambient temperature. Analogous to the heating at 75°C, the main weight loss occurs after the first heating cycle. However, unlike the heating at 75°C, the mass of the composites gradually decreased during the following heating cycles. The absolute value of the slope for SA/MFC 60/40 composite is 1.12 while this for SA/MFC 70/30 composite is 0.85, which indicates the leakage of SA from the MFC surface after every heating step. The

overall mass loss after 5 heating cycles was found to be 12% for SA/MFC 60/40 composite and 11% for SA/MFC 70/30 composite. Noticeable, the slope of the mass loss curve of SA/MFC 60/40 composite is higher than this of SA/MFC 70/30 composite that implies higher mass leakage per heating cycle. Probably, this may be attributed to the fact that in the SA/MFC 60/40 composite SA is spread on the MFC surface in a thinner layer comparing to SA/MFC 70/30 composite, which results in its higher heating rate and, therefore, faster leakage under the same temperature.

In all sets of experiments, the initial mass loss after the first heating cycle was attributed to the leakage of the free SA that can be seen on the SEM and CLSM images (see Figures 1 and 2). This was confirmed by the additional SEM and CLSM measurements of the composites after the heating in the SA leakage test. Figure 8 shows the SEM and CLSM images of SA/MFC 60/40 and SA/MFC 70/30 composites captured after the heating at 75°C and 120°C. As one can see, there are none of any free-standing SA pieces that leaked after the first heating cycle.

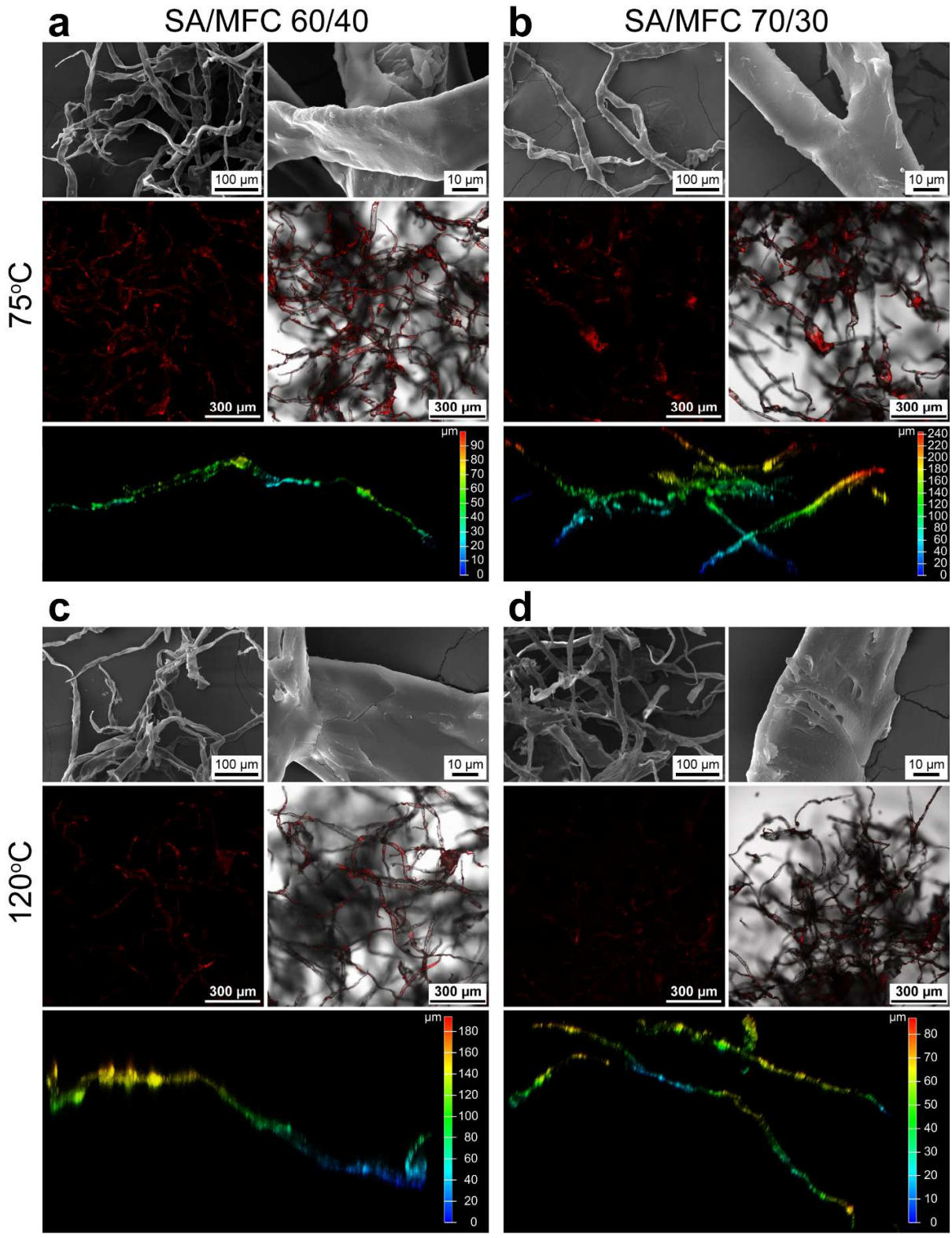
a
SA/MFC 60/40
b
SA/MFC 70/30
75°C
c
d
120°C
100 µm
10 µm
300 µm
µm
90
80
70
60
50
40
30
20
10
0
240
220
200
180
160
140
120
100
80
60
40
20
0

Figure 8. SEM and CLSM images of SA/MFC 60/40 and SA/MFC 70/30 composites after 5 heating cycles at 75°C (a, b) and 120°C (c, d).

The SEM images also confirm that the composites preserve the fibrous structure and the SA remains on the MFC surface. Additionally, the SEM images demonstrate the change in the morphology of the SA layer on the MFC surface. Comparing to the SEM images of the as-prepared composites (see Figure 1c-f), SA appears as a uniform layer after going through the melting and crystallization on the MFC surface. Considering the melting behavior depends on the size and perfection of the crystalline lamellae[24], this explains the shift of the endothermic peak in SA/MFC composites after the first heating/cooling cycle in the thermal cycling test (see Figure 6).

In turn, the CLSM images demonstrate that the fluorescent signal from the SA mixed with Nile Red is following the morphology of cellulose microfibers with a homogeneous distribution of SA over their surface as revealed by the reconstructed 3D images. Additionally, it should be noted that all fluorescent CLSM images were captured under the same microscope settings. However, there is an obvious difference in the fluorescence intensity between the initial composite fibers and the composite fibers after the thermal treatment. This can be related to the thermochromic properties of Nile Red dye, which is known to have a blue shift of emission with the growth of temperature [25].

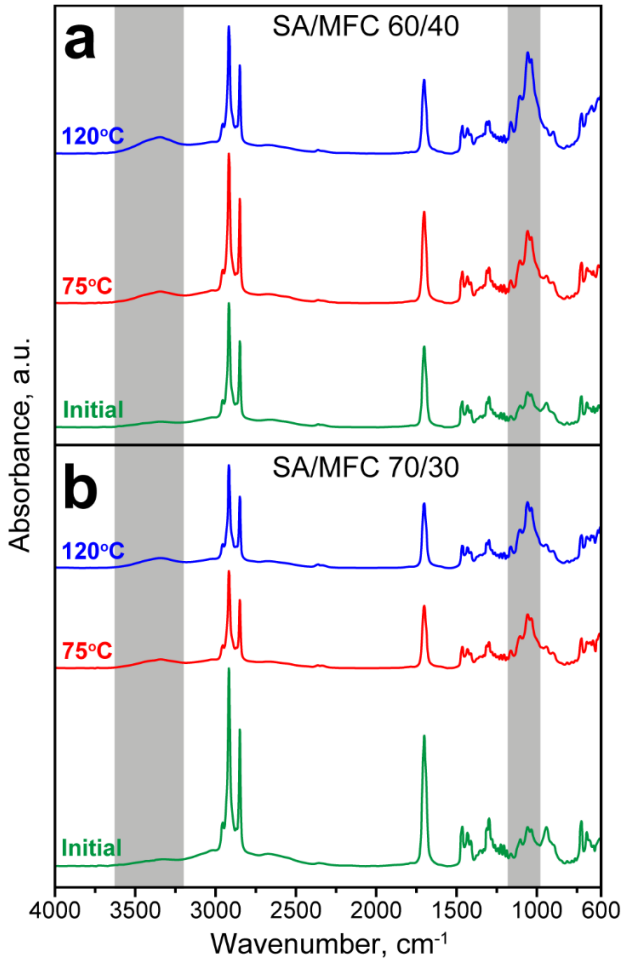

Figure 9. FTIR spectra of SA/MFC 60/40 (a) and SA/MFC 70/30 (b) composites before and after heating at 75°C and 120°C. The grey stripes indicate the absorption bands corresponding to MFC.

The additional confirmation of the presence of SA on the MFC surface after thermal treatment was provided by the FTIR measurements (Figure 9). The FTIR spectra of both SA/MFC 60/40 and SA/MFC 70/30 composites have the peaks inherent to SA and MFC and the heating up to 75°C and 120°C did not result in new chemical bonding in their structure. It is worth noting that the intensity of the peaks corresponding to the absorbance by hydroxyl groups (3600 – 3150 cm^{-1}) and cellulose ring (1200 – 1000 cm^{-1}) is growing with the temperature of composite thermal treatment toward the intensity of characteristic peaks of SA, which is the most obvious in compassion with

the peak at 1700 cm^{-1} and the peaks in the 3000 – 2800 cm^{-1} band. This can be attributed to the change of the SA/MFC ratio in the composite structure due to the leakage of SA. For instance, heating at 75°C resulted in moderate mass loss related to the leakage of the free-standing SA, which, in turn, led to the moderate growth of MFC absorption. The heating at 120°C resulted in more prominent weight loss due to the further leakage of the SA from the MFC surface, and, therefore, the intensity of MFC absorption had grown as well.

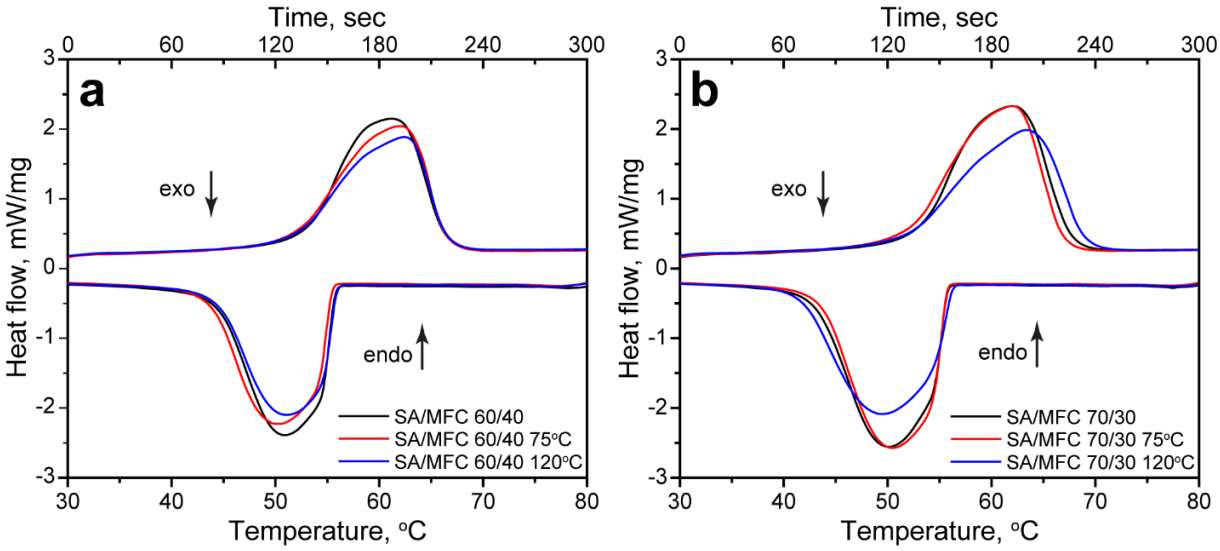

Figure 10. The melting and freezing curves of SA/MFC 60/40 (a) and SA/MFC 70/30 (b) composites before and after heating at 75°C and 120°C.

Finally, the effect of the SA leakage after the shape stability test on the thermal energy storage performance of the SA/MFC composites was evaluated with DSC. Figure 10 shows the comparison of DSC curves of the initial SA/MFC 60/40 and SA/MFC 70/30 composites and the DSC curves measured from these composites after 5 heating cycles at 75°C and 120°C. For SA/MFC 60/40 composite, the leakage of the free-standing SA after heating at 75°C resulted in a negligible reduction of the melting and freezing enthalpies by 2% (the particular values are listed in Table 4). In turn, the 5 heating cycles at 120°C, which were associated with partial desorption

of SA from the MFC, led to the more significant reduction of melting and freezing enthalpies by 12% and 11%, respectively. For SA/MFC 70/30 composite, heating at 75°C resulted in almost the same reduction of the melting and freezing enthalpies by 1%, while the heating at 120°C led to a decrease in melting and freezing enthalpies only by 9%. The smaller decrease of phase transition enthalpies of SA/MFC 70/30 composite comparing to this of SA/MFC 60/40 composite can be related to their lower mass loss as revealed by the mass measurements. Additionally, the SA/MFC 70/30 composite demonstrated a prominent shift of initial and final peak temperatures along with the shape shift of the endothermic and exothermic peaks, which indicates a change in the dynamics of melting and freezing of the SA layer on the MFC surface. This may be associated with a change of the conformation of the SA layer on the MFC surface.

The DSC curves measured after the shape stability test allow one to figure out more accurate values of SA loading ratio, loading efficiency, and thermal storage capability disregarding the contribution of unabsorbed SA. For SA/MFC 60/40 composite after 5 heating cycles at 75°C, the loading ratio and loading efficiency were 59% and 58%, respectively. In turn, for SA/MFC 70/30 composite, the loading ratio and loading efficiency were recalculated to be 69% and 68%, respectively. Predictably, the leakage of the free SA resulted in the reduction of loading ratio and loading efficiency as was expected due to the decrease in freezing and melting enthalpies of the composites. The thermal storage capability remained the same as for the initial composites.

The heating up to 120°C resulted in the partial leakage of SA from the MFC surface. This led to a more pronounced decrease of melting and freezing enthalpies of SA/MFC composites. Therefore, the heat storage and release performance of the composites also decreased, which is reflected by the loading ratio and loading efficiency values. For SA/MFC 60/40 composite after 5 heating cycles at 120°C, the loading ratio reduced to 53%, and the loading efficiency reduced to

52%. In turn, the SA/MFC 70/30 composite demonstrated a reduction of loading ratio to 64% and reduction of loading efficiency to 63%. Again, the thermal storage capability remained the same as for the initial composites, which means the leakage did not affect the process of phase transitions of SA on the MFC surface. The thermal properties of SA/MFC composites measured after the shape stability test are summarized in Table 4.

Table 4. The summary of the thermal properties of SA/MFC 60/40 and SA/MFC 70/30 composites before and after the material leakage test

Sample	T_M, °C	ΔH_M, J/g	T_F, °C	ΔH_F, J/g	*R*, %	*E*, %	η, %
	Initial						
SA/MFC 70/30	61.5	124.7	51.1	124.5	70	69	99
SA/MFC 60/40	61.4	106.7	50.1	105.9	60	59	98
	5 heating cycles at 75°C						
SA/MFC 70/30	61.9	122.9	50.5	122.7	69	68	99
SA/MFC 60/40	61.9	104.8	50.4	104.01	59	58	98
	5 heating cycles at 120°C						
SA/MFC 70/30	63.4	113.1	49.5	112.8	64	63	99
SA/MFC 60/40	62.4	94.2	51.1	93.2	53	52	98

The experiments on the shape stability demonstrated that the adsorption of the SA on the MFC surface effectively prevents SA leakage when the composite fibers are heated up to a temperature comparable to the melting point of SA as exampled by SA/MFC 60/40 and SA/MFC 70/30

composites. The SEM, CLSM, and FTIR confirm that the SA remains on the MFC surface while the mass loss after the first heating cycle is due to the leakage of the free-standing SA. In this temperature range, the SA/MFC composites remain fairly stable and, what is more important, preserve their thermoregulating performance as revealed by the DSC measurements. The SA/MFC composites demonstrated a loss in shape stability and thermoregulating performance only when heated to a temperature far beyond the melting point of SA (twice as much exceeded in this experiment). This can be avoided in real practice by choosing a proper PCM with a phase transition temperature in the desired range.

Conclusion

In this work, we have demonstrated the preparation of shape-stable composite fibers with thermoregulating properties by simple adsorption of stearic acid from melt on the surface of the microfibrillar cellulose with following mechanical grinding to restore the fibrillar structure. The thermoregulating properties of the composite fibers can be adjusted by varying the mass ratio of the stearic acid and cellulose microfibers. Without any modification of cellulose fibers and employment of additional external stimuli, stearic acid couples with cellulose surface by physical adsorption forming the layer following the fiber morphology, which was confirmed by FTIR, SEM, and CLSM. The resulted composite fibers demonstrate good cycling stability of thermal properties as revealed by DSC analysis. The adsorption of stearic acid on the cellulose surface improves its shape stability and effectively prevents its leakage during phase transitions in case the ambient temperature does not significantly exceed the melting point of stearic acid. However, the adsorption of stearic acid on the cellulose microfibers reduces its thermal stability in comparison to bulk stearic acid according to TGA results due to an increase in effective surface area. Additionally, it should be noted that mechanical grinding results in the formation of free

stearic acid particles along with the composite fibers, which may leak during the phase transition in the appropriate environment leading to a negligible decrease in composite's thermal performance.

We believe that the proposed composite fibers may be used as functional additives and fillers to construction materials and textiles bringing them extended thermoregulating performance and improving their mechanical properties. Within the current study, we have demonstrated the preparation of the stable composite fibers by the example of the adsorption of stearic acid. However, the described approach may be further applied to other fatty acids concerning the desired working temperature range. What is more important, these thermoregulating composites are prepared from sustainable materials without using any harsh chemicals and conditions.

ASSOCIATED CONTENT

The Supporting Information is available free of charge at https://pubs.acs.org. The detailed description of FTIR spectra of MFC and SA.

AUTHOR INFORMATION

Corresponding Author

*Denis V. Voronin – National University of Oil and Gas «Gubkin University», Moscow 119991, Russia; Saratov State University, Saratov 410012, Russia; Email: denis.v.voronin@gmail.com

Author Contributions

The manuscript was written through the contributions of all authors. All authors have given approval to the final version of the manuscript.

Notes

The authors declare no competing financial interest.

ACKNOWLEDGMENT

D. Voronin acknowledges the support of RFBR, project number 19-33-60016. K. Cherednichenko and V. Vinokurov acknowledge the support of the Ministry of Science and Higher Education of the Russian Federation in the framework of the state task in the field of scientific activity; subject number FSZE-2020-0007 (0768-2020-0007).

REFERENCES

(1) Chu, S.; Majumdar, A., Opportunities and challenges for a sustainable energy future. *Nature* **2012**, *488*, 294-303.
(2) Csefalvay, E.; Horvath, I. T., Sustainability Assessment of Renewable Energy in the United States, Canada, the European Union, China, and the Russian Federation. *Acs Sustainable Chemistry & Engineering* **2018**, *6*, 8868-8874.
(3) Li, Z. X.; Al-Rashed, A. A. A. A.; Rostamzadeh, M.; Kalbasi, R.; Shahsavar, A.; Afrand, M., Heat transfer reduction in buildings by embedding phase change material in multi-layer walls: Effects of repositioning, thermophysical properties and thickness of PCM. *Energy Convers. Manage.* **2019**, *195*, 43-56.
(4) Liu, Z.; Liu, Y.; He, B.-J.; Xu, W.; Jin, G.; Zhang, X., Application and suitability analysis of the key technologies in nearly zero energy buildings in China. *Renewable and Sustainable Energy Reviews* **2019**, *101*, 329-345.
(5) Stojiljkovic, M.; Stojiljkovic, S.; Todorovic, B.; Reljic, M.; Savić, S.; Petrovic, S. In *Thermal Energy Storage of Composite Materials Based on Clay, Stearic Acid, Paraffin and Glauber's Salt as Phase Change Materials*, Cham, 2019; Springer International Publishing: Cham, 2019; pp 34-43.
(6) Chandel, S. S.; Agarwal, T., Review of current state of research on energy storage, toxicity, health hazards and commercialization of phase changing materials. *Renewable and Sustainable Energy Reviews* **2017**, *67*, 581-596.
(7) Voronin, D. V.; Ivanov, E.; Gushchin, P.; Fakhrullin, R.; Vinokurov, V., Clay Composites for Thermal Energy Storage: A Review. *Molecules* **2020**, *25*, 26.
(8) Shchukina, E. M.; Graham, M.; Zheng, Z.; Shchukin, D. G., Nanoencapsulation of phase change materials for advanced thermal energy storage systems. *Chem. Soc. Rev.* **2018**, *47*, 4156-4175.
(9) Ngwabebhoh, F. A.; Yildiz, U., Nature-derived fibrous nanomaterial toward biomedicine and environmental remediation: Today's state and future prospects. *J. Appl. Polym. Sci.* **2019**, *136*, 47878.
(10) Bo, S.; Min, Z.; Jing, S.; Zhibin, H.; Pedram, F.; Yonghao, N., Applications of Cellulose-based Materials in Sustained Drug Delivery Systems. *Curr. Med. Chem.* **2019**, *26*, 2485-2501.

(11) Medronho, B.; Lindman, B., Brief overview on cellulose dissolution/regeneration interactions and mechanisms. *Adv. Colloid Interface Sci.* **2015**, *222*, 502-508.
(12) Vikulina, A.; Voronin, D.; Fakhrullin, R.; Vinokurov, V.; Volodkin, D., Naturally derived nano- and micro-drug delivery vehicles: halloysite, vaterite and nanocellulose. *New J. Chem.* **2020**, *44*, 5638-5655.
(13) Betancourt-Jimenez, D.; Youngblood, J. P.; Martinez, C. J., Synthesis and Characterization of Fatty Acid Amides from Commercial Vegetable Oils and Primary Alkyl Amines for Phase Change Material Applications. *Acs Sustainable Chemistry & Engineering* **2020**, *8*, 13683-13691.
(14) Makarem, M.; Lee, C. M.; Kafle, K.; Huang, S.; Chae, I.; Yang, H.; Kubicki, J. D.; Kim, S. H., Probing cellulose structures with vibrational spectroscopy. *Cellulose* **2019**, *26*, 35-79.
(15) Pudney, P. D. A.; Mutch, K. J.; Zhu, S., Characterising the phase behaviour of stearic acid and its triethanolamine soap and acid–soap by infrared spectroscopy. *Phys. Chem. Chem. Phys.* **2009**, *11*, 5010-5018.
(16) Singh, R. K.; Gupta, P.; Sharma, O. P.; Ray, S. S., Homogeneous synthesis of cellulose fatty esters in ionic liquid (1-butyl-3-methylimidazolium chloride) and study of their comparative antifriction property. *Journal of Industrial and Engineering Chemistry* **2015**, *24*, 14-19.
(17) Jandura, P.; Kokta, B. V.; Riedl, B., Fibrous long-chain organic acid cellulose esters and their characterization by diffuse reflectance FTIR spectroscopy, solid-state CP/MAS 13C-NMR, and X-ray diffraction. *J. Appl. Polym. Sci.* **2000**, *78*, 1354-1365.
(18) Zhang, H.; Wang, X.; Wu, D., Silica encapsulation of n-octadecane via sol–gel process: A novel microencapsulated phase-change material with enhanced thermal conductivity and performance. *J. Colloid Interface Sci.* **2010**, *343*, 246-255.
(19) Yu, S.; Wang, X.; Wu, D., Microencapsulation of n-octadecane phase change material with calcium carbonate shell for enhancement of thermal conductivity and serving durability: Synthesis, microstructure, and performance evaluation. *Appl. Energy* **2014**, *114*, 632-643.
(20) Pan, L.; Tao, Q.; Zhang, S.; Wang, S.; Zhang, J.; Wang, S.; Wang, Z.; Zhang, Z., Preparation, characterization and thermal properties of micro-encapsulated phase change materials. *Sol. Energy Mater. Sol. Cells* **2012**, *98*, 66-70.
(21) Ilyas, R. A.; Sapuan, S. M.; Ishak, M. R., Isolation and characterization of nanocrystalline cellulose from sugar palm fibres (Arenga Pinnata). *Carbohydr. Polym.* **2018**, *181*, 1038-1051.
(22) Jandura, P.; Riedl, B.; Kokta, B. V., Thermal degradation behavior of cellulose fibers partially esterified with some long chain organic acids. *Polym. Degrad. Stab.* **2000**, *70*, 387-394.
(23) Menczel, J. D., 4 - Thermogravimetric analysis of fibers. In *Thermal Analysis of Textiles and Fibers*, Jaffe, M.; Menczel, J. D., Eds. Woodhead Publishing: 2020; pp 71-79.
(24) Frone, A. N.; Berlioz, S.; Chailan, J.-F.; Panaitescu, D. M., Morphology and thermal properties of PLA–cellulose nanofibers composites. *Carbohydr. Polym.* **2013**, *91*, 377-384.
(25) Kawski, A.; Kukliński, B.; Bojarski, P., Photophysical properties and thermochromic shifts of electronic spectra of Nile Red in selected solvents. Excited states dipole moments. *Chem. Phys.* **2009**, *359*, 58-64.

SYNOPSIS (Word Style "SN_Synopsis_TOC"). If you are submitting your paper to a journal that requires a synopsis, see the journal's Instructions for Authors for details.